Applied Catalysis B: Environmental 160–161 (2014) 173–178

Contents lists available at ScienceDirect

Applied Catalysis B: Environmental

journal homepage: www.elsevier.com/locate/apcatb

Enhanced visible light-driven hydrogen production from water by a noble-metal-free system containing organic dye-sensitized titanium dioxide loaded with nickel hydroxide as the cocatalyst

Zhiping Yan, Xingxing Yu, Yanyu Zhang, Hongxing Jia, Zijun Sun, Pingwu Du*

Department of Materials Science and Engineering, CAS Key Laboratory of Materials for Energy Conversion, University of Science and Technology of China (USTC), Hefei, 230026, China

ARTICLE INFO

Article history:
Received 3 February 2014
Received in revised form 1 May 2014
Accepted 11 May 2014
Available online 16 May 2014

Keywords:
Transition metal
Photocatalytic
Nickel
Hydrogen production

ABSTRACT

Platinum is an excellent catalyst for hydrogen production but its application is limited by the high cost. In this present paper, a series of noble-metal-free nickel hydroxide/titanium dioxide ($Ni(OH)_2/TiO_2$) nanocomposites have been synthesized and characterized. Photocatalytic hydrogen production was observed in a system containing Eosin Y-sensitized $Ni(OH)_2/TiO_2$ photocatalysts in the presence of triethanolamine (TEOA) as a sacrificial reagent under visible light ($\lambda > 420$ nm). The resulting photocatalysts were well characterized by powder X-ray diffraction (XRD), scanning electron microscopy (SEM), UV–vis spectroscopy (UV–vis), and X-ray photoelectron spectroscopy (XPS). The results revealed that dye-sensitized $Ni(OH)_2/TiO_2$ material has much higher photocatalytic activity than dye-sensitized TiO_2 sample, indicating the important catalytic role of $Ni(OH)_2$. The amount of the loaded cocatalyst significantly affected the photocatalytic activity and the optimal mole ratio of $Ni(OH)_2$ in $Ni(OH)_2/TiO_2$ composite was determined to be 1.0%. The optimal rate of H_2 evolution is about 15.76 μmol h^{-1}, which is about 90 times higher than pure TiO_2 under the same condition. After 5 h of irradiation, the photocatalytic activity of $Ni(OH)_2$ as the cocatalyst for hydrogen evolution is much higher than other first-row transition metal based oxide/hydroxide materials, such as cobalt oxide (CoO_x), cobalt hydroxide ($Co(OH)_2$), nickel oxide (NiO_x), ferric hydroxide ($Fe(OH)_3$) and copper hydroxide ($Cu(OH)_2$) on the surface of TiO_2 semiconductor.

1. Introduction

To split water into hydrogen and oxygen utilizing solar energy is an ideal way to produce renewable and clean hydrogen energy, which is considered as a promising approach toward solving worldwide energy and environmental issues [1–7]. Visible light-driven photocatalysis using semiconductor materials has been attracting extensive attention in the past decades since the Honda–Fujishima effect discovered in 1972 [8–10]. So far, many semiconductor materials have been explored and shown exciting catalytic activity, such as titanium dioxide (TiO_2) [11–18], cadmium sulfide (CdS) [19,20], reduced graphene oxide (RGO) [21–23], graphitic carbon nitride (g-C_3N_4) [24–27], $AgPO_4$ [28] etc. TiO_2 is a good candidate for possible applications because of its excellent properties, including nontoxicity, low-cost, robust physical and chemical properties. However, titanium dioxide can only utilize the small ultraviolet fraction of solar light due to the large intrinsic bandgap of titanium dioxide (3.0 eV for rutile and 3.2 eV for anatase). UV light accounts for only a small proportion (4%) of the solar energy in comparison with visible light (43%), resulting in a poor efficiency in solar energy conversion. Therefore, if the optical response of the photocatalysts can shift from UV to visible light region, it would produce a positive effect on improving photocatalytic activity. Dye-sensitization of the photocatalysts could provide a good approach to improve the light-absorption properties [17,29,30].

In a photocatalytic water splitting system, the photogenerated electrons and holes could easily recombine if there are no suitable active sites on the surface of semiconductors. Proper cocatalysts loaded on the semiconductors could improve the photocatalytic processes. For example, depositing platinum (Pt) on TiO_2 surface can greatly increase the rate of hydrogen production due to great capability to accept electrons by Pt cocatalyst [31–35]. The drawback of this noble metal catalyst, however, is its scarcity and

* Corresponding author at: Department of Materials Science and Engineering, CAS Key Laboratory of Materials for Energy Conversion, University of Science and Technology of China (USTC), Hefei, 230026, China. Tel.: +86 551 63606207; fax: +86 551 63606207.
E-mail address: dupingwu@ustc.edu.cn (P. Du).

http://dx.doi.org/10.1016/j.apcatb.2014.05.017
0926-3373/

cost. Therefore, it's essential to search earth-abundant elements to replace noble metal based cocatalysts [5,36,37]. It is also well-known that loading metallic oxides and metallic hydroxides on the surface of TiO_2 could create electrons and holes sinks, which enhances the separation of charge carriers and inhibits the recombination of electron and hole pairs, such as SnO_2 [38,39], ZnO [40], CoO_x [41], Co_3O_4 [42,43], and $Cu(OH)_2$ [44].

Herein, we report a highly active noble-metal-free system for visible light-driven hydrogen production from water containing Eosin Y dye-sensitized $Ni(OH)_2/TiO_2$ and triethanolamine (TEOA) as a sacrificial reagent. The results show that the loading of $Ni(OH)_2$ and adding EY dye play an important role on photocatalytic activity for visible light. The effects of different amount of nickel hydroxide and the pH values on the performance of photocatalytic activity were investigated. Furthermore, the mechanism of the process for the photocatalyst composite was also discussed. The results demonstrate that the as-prepared dye-sensitized $Ni(OH)_2/TiO_2$ composite can serve as a promising photocatalyst for hydrogen evolution in visible light region.

2. Experimental

2.1. Materials

All the chemicals, including sodium hydroxide (NaOH), hydrochloric acid (HCl), Degussa P25, nickel nitrate hexahydrate ($Ni(NO_3)_2{\cdot}6H_2O$), cobalt nitrate hexahydrate ($Co(NO_3)_2{\cdot}6H_2O$), ferric chloride ($FeCl_3$), copper chloride dihydrate ($CuCl_2{\cdot}2H_2O$), triethanolamine (TEOA), Eosin Y dye and ethanol, were all commercially available (Aldrich or Acros, analytical grade) and used without further purification.

2.2. Synthesis of the photocatalysts

Synthesis of $Ni(OH)_2/TiO_2$ composites: 1.0 g Degussa P25 was dispersed in 25 mL 1.0 M NaOH solution, and then a calculated amount of $Ni(NO_3)_2{\cdot}6H_2O$ was added and stirred for 24 h. After that, the mixture was centrifuged, washed by distilled water and anhydrous ethanol for three times, and dried at 353 K overnight. The product was collected and ground into powder. This sample was denoted as $Ni(OH)_2/TiO_2$ (the mole ratios of $Ni(OH)_2$ with $Ni(OH)_2/TiO_2$ were 0%, 0.25%, 0.5%, 1.0%, 2.0%, 4.0%, 50%, respectively, which were denoted as Ni-NT0, Ni-NT0.25, Ni-NT0.5, Ni-NT1, Ni-NT2, Ni-NT4, Ni-NT50). The synthetic procedures for $Co(OH)_2/TiO_2$, $Cu(OH)_2/TiO_2$, $Fe(OH)_3/TiO_2$ were the same as that for synthesis of $Ni(OH)_2/TiO_2$ except that $Co(NO_3)_2{\cdot}6H_2O$, $CuCl_2{\cdot}2H_2O$ and $FeCl_3$ were used to replace the nickel salt. NiO_x/TiO_2 and CoO_x/TiO_2 composites were synthesized by heating the $Ni(OH)_2/TiO_2$ and $Co(OH)_2/TiO_2$ samples, respectively, to 673 K for 2 h under air in an oven.

2.3. Characterization

The crystal phases and phase compositions of the composite photocatalysts were determined by powder X-ray diffraction (XRD, D/max-TTR III) using graphite monochromatized Cu Kα radiation of 1.54178 Å, operating at 40 kV and 200 mA. The scanning rate was 5° min^{-1} from 20° to 70° in 2θ. SEM images were obtained with a SIRION200 Schottky field emission scanning electron microscope (SFE-SEM) and the morphologies of the samples were also determined by high-resolution transmission electron microscopy (HR-TEM, JEM-2010) equipped with an electron diffraction (ED) attachment with an acceleration voltage of 200 kV. X-ray photoelectron spectroscopy (XPS) measurement was done by an ESCALAB 250 X-ray photoelectron spectrometer. The photoluminescence spectra were recorded on a FluoroMax-4 spectrometer, and transient photoluminescence (PL) decay spectra were obtained on a FluoroHub-B spectrometer at room temperature.

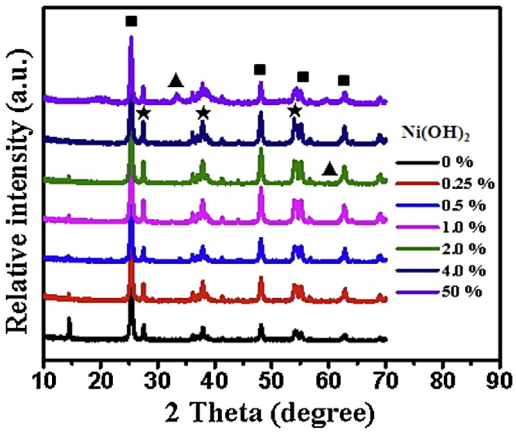

Fig. 1. Powder X-ray diffraction (XRD) patterns of Ni-NT0, Ni-NT0.25, Ni-NT0.5, Ni-NT1, Ni-NT2, Ni-NT4, Ni-NT50 samples.

2.4. Photocatalytic hydrogen production

The photocatalytic hydrogen production experiments were performed in a 50 mL flask at ambient temperature using a 300 W Xe lamp equipped with UV cut off filter (λ > 420 nm). Hydrogen gas was measured by gas chromatography (SP-6890, nitrogen as a carrier gas) equipped with thermal conductivity detector (TCD). In a typical photocatalytic experiment, 10 mg of the photocatalyst and a calculated amount of Eosin Y dye were mixed in 20 mL of TEOA-H_2O solution (5%, v/v) by ultrasonicating for 10 min. All the photocatalysts used in this paper were 10 mg. The pH values of the reaction solution were adjusted by addition of 2 M HCl or NaOH. Before each experiment, the suspension was purged with nitrogen for 15 min to remove air. After that, 5 mL of methane was added to serve as the internal standard. During the photocatalytic reaction, the reactor was tightly sealed to avoid a gas exchange.

3. Results and discussion

3.1. X-ray diffraction analyses

Fig. 1 shows powder X-ray diffraction (XRD) patterns of the $Ni(OH)_2/TiO_2$ composites with variable $Ni(OH)_2$ contents, as well as pure TiO_2. All the reflections from pure TiO_2 can be indexed to the anatase phase and rutile phase. The peaks marked "■" are the anatase form and those marked "⋆" are the rutile form. The XRD patterns reveal that TiO_2 nanoparticles in the anatase phase with typical peaks at 2θ = 25.1°, 48.1°, 55.2° and 62.5°, which correspond to (1 0 1), (2 0 0), (2 1 1) and (2 0 4) planes, respectively. The remaining peaks at 2θ = 27.4°, 37.1° and 54.1° can be indexed to the reflection from (1 1 0), (1 0 1) and (2 1 1) planes of the rutile phase of TiO_2 [35,45,46]. When the mole ratios of $Ni(OH)_2$ in $Ni(OH)_2/TiO_2$ composites vary from 0.25% to 4.0%, all the typical P25 XRD patterns are remained and only slight characteristic diffraction peaks $Ni(OH)_2$ could be observed at 2θ = 34.1° and 59.0°, corresponding to the reflection from (1 0 1) and (1 1 0) plane, respectively [47]. The result also suggests that no $Ni(OH)_2$ clusters incorporate into the lattice of TiO_2 to change its diffraction peaks. Moreover, when the ratio of $Ni(OH)_2$ reaches 50%, a big diffraction peak at 2θ = 34.1° is clearly observed which marked with "▲", corresponding to (1 0 1) plane diffraction of $Ni(OH)_2$ [47].

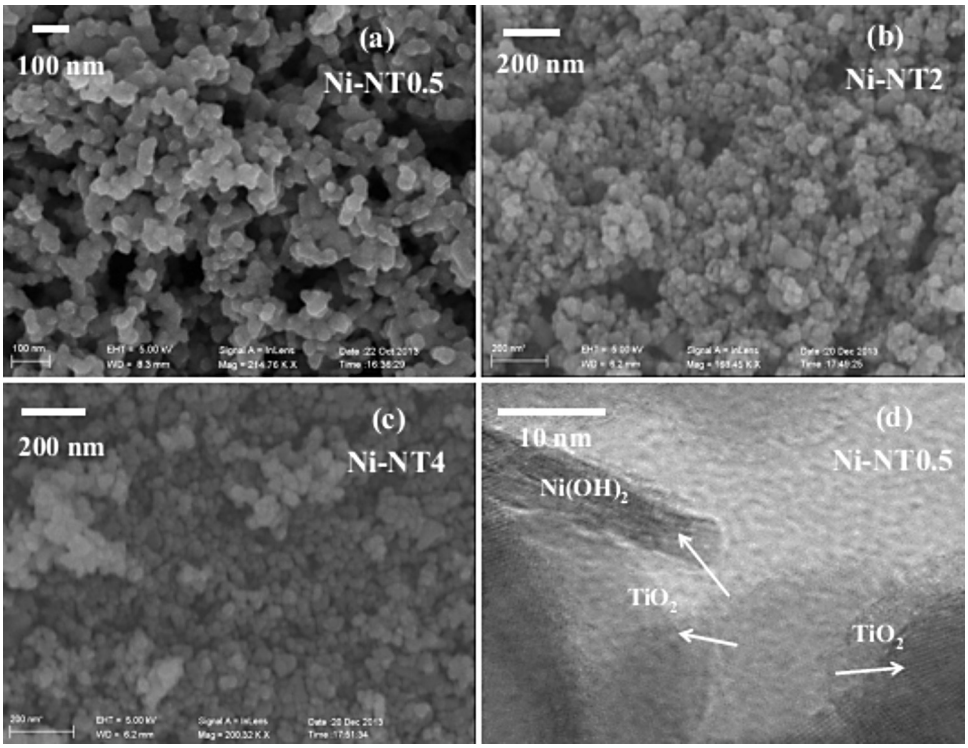

Fig. 2. Scanning electron microscope (SEM) images of Ni-NT0.5, Ni-NT2, Ni-NT4 samples and high-resolution transmission electron microscope (HR-TEM) image of Ni-NT0.5 sample.

3.2. SEM and XPS characterization

Scanning electron microscopy (SEM) images are taken to analyze the morphologies of the samples, as displayed in Fig. 2a–c (Ni-NT0.5, Ni-NT2 and Ni-NT4 as the examples). It can be observed that the as-prepared samples show good dispersity and uniformity, and the average diameter of particles is about 20–30 nm. To probe the $Ni(OH)_2$ species on TiO_2, high resolution transmission electron microscopy (HR-TEM) was used to measure Ni-NT0.5 sample (Fig. 2d). The image clearly shows the presence of $Ni(OH)_2$ material attached onto TiO_2 nanoparticles.

The surface composite and element valence states of the as-prepared Ni-NT0.5 were determined by X-ray photoelectron spectroscopy (XPS) analysis. It shows the materials mainly contain Ti, C, O and Ni elements in the survey scan (Fig. 3a). In the XPS spectrum of Fig. 3b, the binding energy of Ni $2p_{3/2}$ centered at 855.78 eV is the typical Ni^{2+} phase of $Ni(OH)_2$ [48]. The peak at 873.18 eV is assigned to the binding energy of Ni^{2+} $2p_{1/2}$ [49,50]. The peak at 285.13 eV is the characteristic peak of C 1s, which is used as the standard peak.

3.3. Photophysical properties

To evaluate the visible light-absorption properties, we studied the absorption spectra of the EY, EY-TEOA, EY-$Ni(OH)_2$/TiO_2 and EY-TEOA-$Ni(OH)_2$/TiO_2 materials, as shown in Fig. 4. In the visible region, all four samples exhibit similar absorption bands in the visible region, maximized at 523 nm, corresponding to the intrinsic absorption of EY [51,52]. The extinction coefficient of EY at 523 nm is about $8.0 \times 10^4\ M^{-1}\ cm^{-1}$ in water at pH 9. Moreover, there is big change for the absorption baselines of EY-$Ni(OH)_2$/TiO_2 and EY-TEOA-$Ni(OH)_2$/TiO_2 diluted solutions, probably due to the small absorption/scattering of $Ni(OH)_2$/TiO_2 nanomaterials in solution.

To examine the effect of $Ni(OH)_2$ loading on TiO_2 particles, photoluminescence (PL) spectroscopy was used to characterize the photophysical properties. Fig. 5 shows a comparison of PL

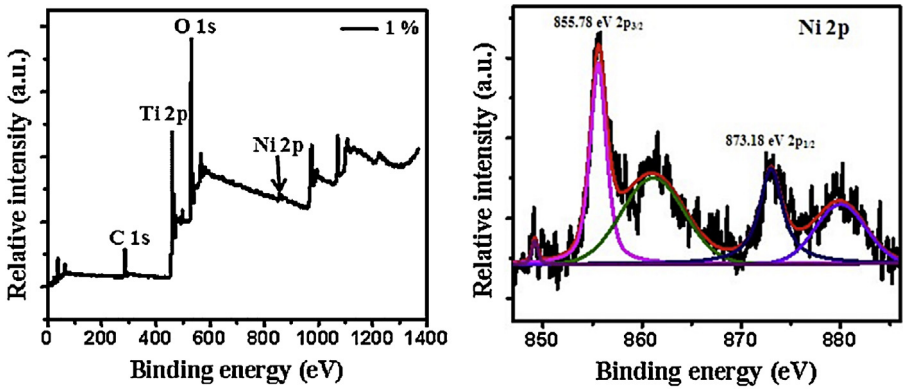

Fig. 3. (a) XPS survey spectrum of Ni-NT1 sample containing 1% $Ni(OH)_2$. (b) XPS spectra of Ni 2p acquired from Ni-NT1 sample.

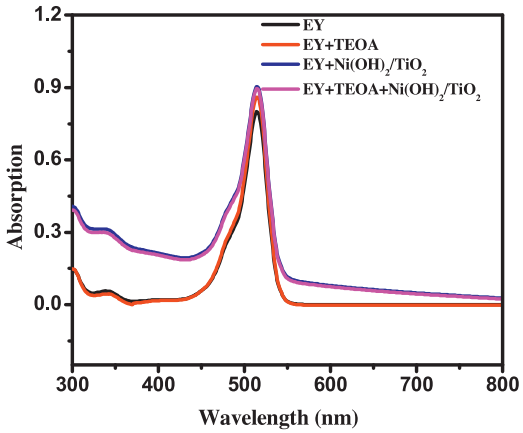

Fig. 4. UV–vis spectra of EY, EY-TEOA, EY-Ni(OH)$_2$/TiO$_2$, EY-TEOA-Ni(OH)$_2$/TiO$_2$ aqueous solutions. Test conditions: 1.0×10^{-5} M EY, 1.0×10^{-5} M Ni(OH)$_2$/TiO$_2$, 1.0×10^{-5} M TEOA solution, pH 9.

spectra of pure TiO$_2$ and Ni-NT1 samples under the same condition, excited at 380 nm. The shape of two PL spectra is quite similar. However, considerable PL quenching is observed when Ni(OH)$_2$ is loaded on the surface of TiO$_2$, indicating that Ni(OH)$_2$ could accept electrons from TiO$_2$ and promote fast electron–hole separation under visible light irradiation. Therefore, Ni(OH)$_2$ could serve as the electron acceptor and transporter, which will reduce the fast recombination of electrons and holes, and further increase the efficiency of photocatalysis. The time-resolved PL decays further indicate that the PL lifetime of EY-Ni(OH)$_2$/TiO$_2$ solution is shorter than EY-TiO$_2$ in solution, excited at 450 nm (Fig. 6). The PL lifetime of EY-Ni(OH)$_2$/TiO$_2$ is 0.23 ns and that of EY-TiO$_2$ solution is 1.13 ns, which confirms that the decrease of the PL lifetime within EY-Ni(OH)$_2$/TiO$_2$ solution, corresponding to the fast transfer of electrons from EY to Ni(OH)$_2$/TiO$_2$.

3.4. Visible light-driven hydrogen production

The photocatalytic activities of Ni(OH)$_2$/TiO$_2$ composites for hydrogen production were evaluated under visible light irradiation ($\lambda > 420$ nm) using TEOA as a sacrificial electron donor. As shown in Fig. 7, the photocatalytic activity for H_2 generation under visible irradiation is remarkably enhanced by attaching Ni(OH)$_2$ nanomaterials onto TiO$_2$ particles. The corresponding H_2 evolution rate of Ni-NT0.5 catalyst is 7.74 μmol h^{-1}. For comparison, pure TiO$_2$ sample was used for hydrogen production under the same condition.

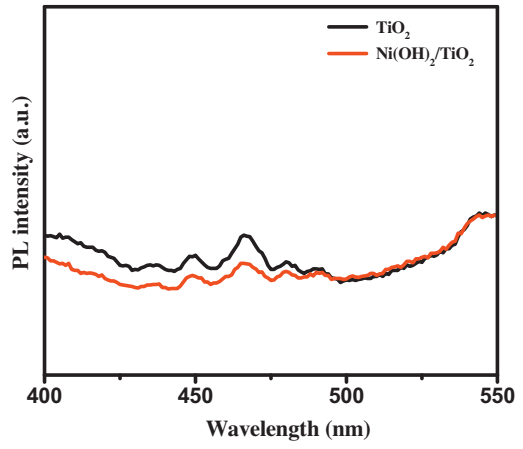

Fig. 5. Comparison of photoluminescence (PL) spectra of solid powders of TiO$_2$ and Ni(OH)$_2$/TiO$_2$ (1.0% Ni(OH)$_2$) composite with excitation wavelength at 380 nm.

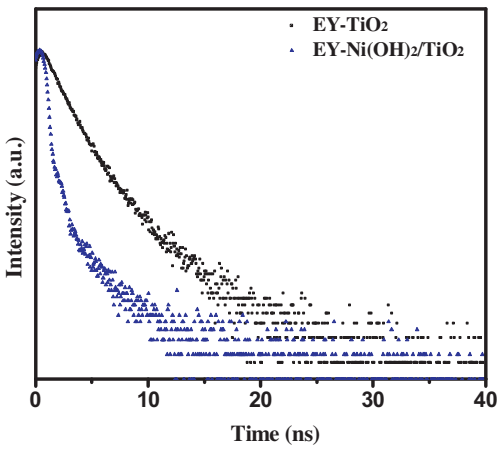

Fig. 6. Comparison of the PL decay curves for EY-TiO$_2$ and EY-Ni(OH)$_2$/TiO$_2$ in diluted solutions. Test conditions: 1.0×10^{-5} M EY, 1.0×10^{-5} M TiO$_2$, 1.0×10^{-5} M Ni-NT1 solution; excitation wavelength, 390 nm.

No appreciable H_2 gas was detected in the absence of Ni(OH)$_2$, indicating that Ni(OH)$_2$ serves as an efficient cocatalyst to improve the photocatalytic activity.

Fig. 8 shows the hydrogen evolution activity of using Ni-NT0.5 in EY solution under different pH values from 7 to 10, irradiated by visible light ($\lambda > 420$ nm). The result shows that pH has a great effect on hydrogen production and the highest rate of hydrogen production was achieved at pH 9. The rates of H_2 evolution were 0.17, 2.16, 7.74 and 4.53 μmol h^{-1} when the reaction was run at pH 7, 8, 9 and 10, respectively. When the pH is below 7, the significant decrease of H_2 formation likely results from protonation of TEOA, which might render TEOA an ineffective sacrificial donor. When pH is higher, the driving force for hydrogen production is decreased ($2H^+ + 2e \rightarrow H_2$, $E = -0.059$ pH V vs. NHE). The pH dependence is a common phenomenon in many hydrogen production systems [53,54].

For comparison, different first-row transition metal based hydroxides and oxides such as Co(OH)$_2$, Fe(OH)$_3$, Cu(OH)$_2$, CoO$_x$ and NiO$_x$ were used as the cocatalysts for photocatalytic hydrogen production. These cocatalysts were loaded on the surface of TiO$_2$, and all the ratios of cocatalysts are 0.5%. As shown in Fig. 9, it is demonstrated that Ni(OH)$_2$ is the best cocatalyst for H_2 evolution among all the samples. The rates of H_2 evolution were 0.34, 1.59, 3.70, 0.37, 7.74, 0.74 and 5.86 μmol h^{-1} for CoO$_x$, Co(OH)$_2$, NiO$_x$,

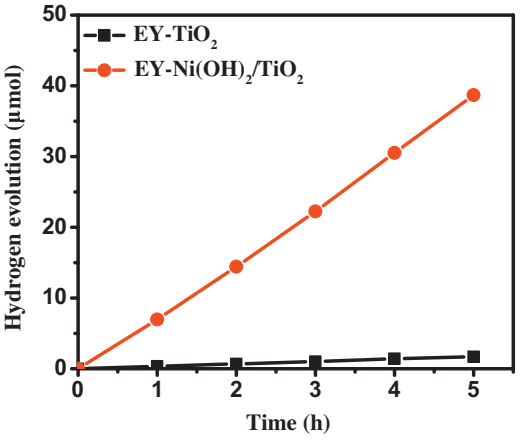

Fig. 7. The profiles of photocatalytic hydrogen production in 20 mL aqueous solution containing 1 mL TEOA with 0.01 g of Ni-NT0.5 and Ni-NT0 samples, respectively. Using 300 W xenon arc lamp as the light source and a cut filter to cut the photons below 420 nm.

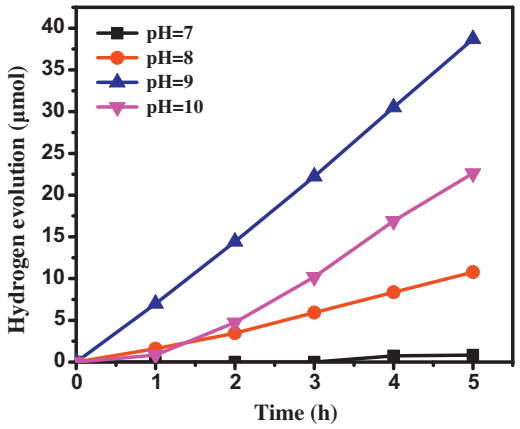

Fig. 8. Hydrogen production from Ni-NT0.5 in EY solution at several pHs (pH 7, 8, 9, 10). Using 300 W xenon arc lamp as the light source and a cut filter to cut the photons below 420 nm.

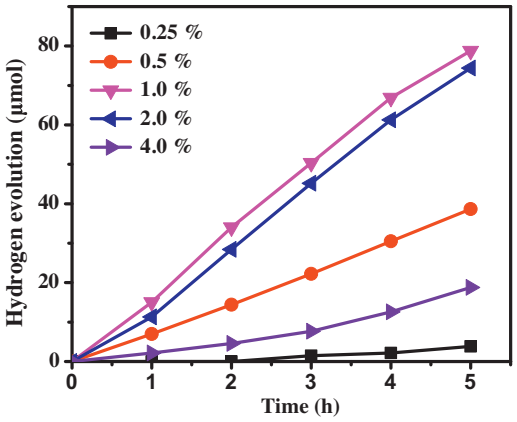

Fig. 10. The profiles of photocatalytic hydrogen production from 20 mL aqueous solution containing 1 mL TEOA with 0.01 g of Ni-NT0.25, Ni-NT0.5, Ni-NT1, Ni-NT2, Ni-NT4 samples, respectively. Using 300 W xenon arc lamp as the light source and a cut filter to cut the photons below 420 nm.

$Ni(OH)_2$, $Fe(OH)_3$ and $Cu(OH)_2$, respectively. The results clearly indicated that $Ni(OH)_2$ could function as a more efficient cocatalyst for photocatalytic hydrogen production from water than other first-row transition metal hydroxides and metal oxides as mentioned above.

The effect of different ratios of $Ni(OH)_2$ loaded on TiO_2 was further studied for photocatalytic hydrogen production, as shown in Fig. 10. All the catalyst composites exhibited enhanced activity for hydrogen production when irradiated by visible light from the ratio of 0.25–4.0%. The photocatalysts Ni-NT1 produced the highest amount of hydrogen gas during the photocatalytic reaction and the average rate of hydrogen evolution reached to 15.76 μmol h^{-1}, which is 90 times higher than the system containing no $Ni(OH)_2$. The average rates of hydrogen evolution of Ni-NT0.25, Ni-NT0.5, Ni-NT2, Ni-NT4 were 0.77, 7.74, 14.88 and 3.76 μmol h^{-1}, respectively. Higher ratio of $Ni(OH)_2$ loading did not lead to an increase in the H_2 evolution, as evidenced by the samples Ni-NT2 and Ni-NT4. Large excess percentage of $Ni(OH)_2$ possibly led to shield the active sites on the surface of semiconductor and therefore decrease the catalytic activity.

Besides its good activity, the stability of a photocatalyst is also important for photocatalysis. To demonstrate the stability of the $Ni(OH)_2/TiO_2$ composite, we carried out photocatalytic reaction using Ni-NT1 as an example. The reaction system was evaluated every 3 h as one cycle. The average rates of hydrogen evolution of first, second, third and fourth cycle were 5.62, 5.42, 5.35 and 5.30 μmol h^{-1}. No significant decrease of H_2 evolution is observed after 12 h, as shown in Fig. 11, indicating the good stability of the present system for photocatalytic hydrogen production. By examining the absorption spectra of EY dye after 12 h of visible light irradiation, it is found that the concentration of EY decreased from 1.0×10^{-5} M to 0.35×10^{-5} M. The decomposition of EY did not significantly affect the photocatalytic activity, indicating such a concentration is probably not the rate-determining factor for hydrogen production in the present system.

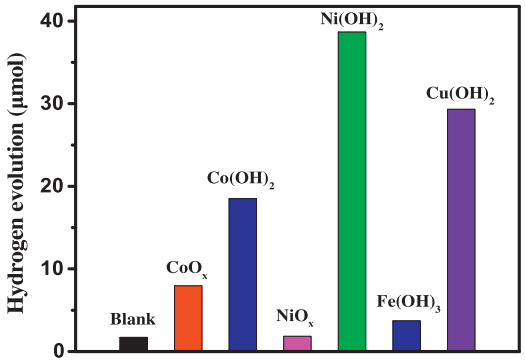

Fig. 9. Hydrogen production from CoO_x, $Co(OH)_2$, NiO_x, $Ni(OH)_2$, $Fe(OH)_3$ and $Cu(OH)_2$, respectively in EY solution at pH 9 for 5 h. Using 300 W xenon arc lamp as the light source and a cut filter to cut the photons below 420 nm.

3.5. Proposed mechanism

Based on what has been observed and discussed above, the photocatalytic mechanism using EY-$Ni(OH)_2/TiO_2$ material is proposed and shown in Scheme 1. First, the molecules of EY dye absorb the photons from visible light to generate the excited states, followed by intersystem crossing to populate the triplet excited states [55]. Subsequent electron transfer takes place from the excited EY to the conduction band of TiO_2 particles. Due to the efficient visible light absorption capability of EY dye, the activity of EY-$Ni(OH)_2/TiO_2$ is superior to $Ni(OH)_2/TiO_2$ without the EY dye. Furthermore, the water molecules absorb on the TiO_2 accept the electrons on the TiO_2 surfaces coming from EY dye and are reduced to hydrogen [33]. When $Ni(OH)_2$ is loaded on TiO_2, the charge separation could be further enhanced when electrons are efficiently collected by $Ni(OH)_2$, which catalyzes the reduction of proton to hydrogen with these photogenerated electrons.

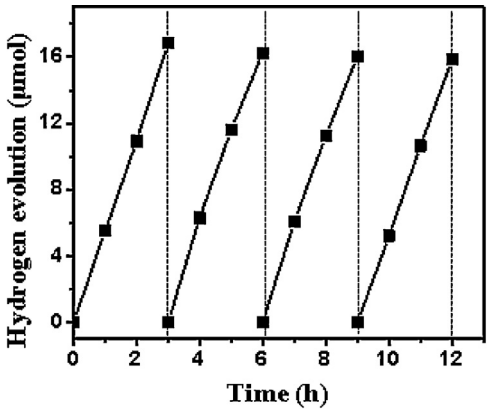

Fig. 11. Hydrogen production profile of Ni-NT1 as the function of time from an aqueous solution containing TEOA reagent evacuated per 3 h without renewing the sacrificial agents. Using 300 W xenon arc lamp as the light source and a cut filter to cut the photons below 420 nm.

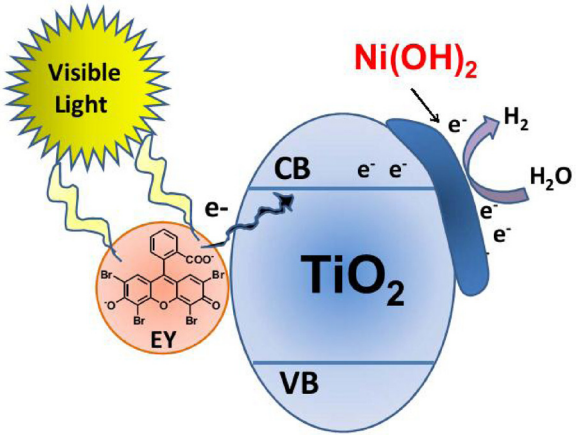

Scheme 1. Mechanism for the photocatalytic hydrogen production over EY-sensitized $Ni(OH)_2/TiO_2$.

4. Conclusion

In conclusion, the photocatalytic H_2 production on TiO_2 under visible light ($\lambda > 420$ nm) can be significantly enhanced by adding EY dye as a photosensitizer and loading $Ni(OH)_2$ as a cocatalyst in the presence of TEOA as a sacrificial reagent. The optimal mole ratio of $Ni(OH)_2$ loading is determined to be 1.0%, and the average rate of hydrogen evolution is 15.76 μmol h^{-1}, which is about 90 times higher than the sample containing no $Ni(OH)_2$ cocatalyst under the same condition. The photocatalytic activity for hydrogen production by $Ni(OH)_2/TiO_2$ composite is much higher than that other first-row transition metal based oxide/hydroxide materials, such as CoO_x, $Co(OH)_2$, NiO_x, $Fe(OH)_3$ and $Cu(OH)_2$ on the surface of TiO_2 nanoparticles under the same condition. The high photocatalytic activity of $Ni(OH)_2/TiO_2$ samples should be attributed to the efficient separation of electron–hole pairs in semiconductor composites. We demonstrate in this work that dye-sensitized TiO_2 loaded with $Ni(OH)_2$ as the cocatalyst is an attractive way for catalytic H_2 production by visible light.

Acknowledgments

This work was financially supported by the National Natural Science Foundation of China (21271166), the Fundamental Research Funds for the Central Universities (WK2060140015 and WK2060190026), the Program for New Century Excellent Talents in University (NCET), and the Thousand Young Talents Program.

References

[1] H.B. Gray, Nature 1 (2009) 7.
[2] N.S. Lewis, D.G. Nocera, Proc. Natl. Acad. Sci. U.S.A. 103 (2006) 15729–15735.
[3] T.J. Meyer, Acc. Chem. Res. 22 (1989) 163–170.
[4] A.J. Bard, M.A. Fox, Acc. Chem. Res. 28 (1995) 141–145.
[5] P. Du, R. Eisenberg, Energy Environ. Sci. 5 (2012) 6012–6021.
[6] L. Duan, L. Tong, Y. Xu, L. Sun, Energy Environ. Sci. 4 (2011) 3296–3313.
[7] M. Woodhouse, B.A. Parkinson, Chem. Soc. Rev. 38 (2009) 197–210.
[8] A. Fujishima, K. Honda, Nature 238 (1972) 37–38.
[9] D.G. Nocera, Acc. Chem. Res. 45 (2012) 767–776.
[10] J.P. McEvoy, G.W. Brudvig, Chem. Rev. 106 (2006) 4455–4483.
[11] H. Liu, H.T. Ma, X.Z. Li, W.Z. Li, M. Wu, X.H. Bao, Chemosphere 50 (2003) 39–46.
[12] Q.J. Xiang, J.G. Yu, M. Jaroniec, J. Am. Chem. Soc. 134 (2012) 6575–6578.
[13] T. Miwa, S. Kaneco, H. Katsumata, T. Suzuki, K. Ohta, S.C. Verma, K. Sugihara, Int. J. Hydrogen Energy 35 (2010) 6554–6560.
[14] Y. Cong, J.L. Zhang, F. Chen, M. Anpo, J. Phys. Chem. C 111 (2007) 6976–6982.
[15] J.G. Yu, Y. Hai, B. Cheng, J. Phys. Chem. C 115 (2011) 4953–4958.
[16] T. Kamegawa, H. Seto, S. Matsuura, H. Yamashita, ACS Appl. Mater. Interfaces 4 (2012) 6635–6639.
[17] T. Kamegawa, S. Matsuura, H. Seto, H. Yamashita, Angew. Chem. Int. Ed. 52 (2013) 916–919.
[18] H. Yamashita, K. Maekawa, Y. Nakatani, J.J. Park, M. Anpo, Chem. Lett. 32 (2003) 930–931.
[19] X. Zong, G.P. Wu, H.J. Yan, G.J. Ma, J.Y. Shi, F.Y. Wen, L. Wang, C. Li, J. Phys. Chem. C 114 (2010) 1963–1968.
[20] N. Zhang, M.Q. Yang, Z.R. Tang, Y.J. Xu, J. Catal. 303 (2013) 60–69.
[21] P.D. Tran, S.K. Batabyal, S.S. Pramana, J. Barber, L.H. Wong, S.C.J. Loo, Nanoscale 4 (2012) 3875–3878.
[22] Z.G. Mou, S.L. Yin, M.S. Zhu, Y.K. Du, X.M. Wang, P. Yang, J.W. Zheng, C. Lu, Phys. Chem. Chem. Phys. 15 (2013) 2793–2799.
[23] Y.J. Chen, H. Ge, L. Wei, Z.H. Li, R.S. Yuan, P. Liu, X.Z. Fu, Catal. Sci. Technol. 3 (2013) 1712–1717.
[24] X.J. Bai, L. Wang, R.L. Zong, Y.F. Zhu, J. Phys. Chem. C 117 (2013) 9952–9961.
[25] L. Ge, C.C. Han, Appl. Catal., B 117 (2012) 268–274.
[26] J.H. Liu, T.K. Zhang, Z.C. Wang, G. Dawson, W. Chen, J. Mater. Chem. 21 (2011) 14398–14401.
[27] Y.W. Zhang, J.H. Liu, G. Wu, W. Chen, Nanoscale 4 (2012) 5300–5303.
[28] Y. Bi, S. Ouyang, N. Umezawa, J. Cao, J. Ye, J. Am. Chem. Soc. 133 (2011) 6490–6492.
[29] M. Gratzel, Coord. Chem. Rev. 111 (1991) 167–174.
[30] B. O'Regan, M. Grätzel, Nature 353 (1991) 737.
[31] J. Kiwi, M. Grätzel, J. Am. Chem. Soc. 101 (1979) 7214–7217.
[32] J. Kiwi, M. Grätzel, Nature 281 (1979) 657–658.
[33] M. Grätzel, Acc. Chem. Res. 14 (1981) 376–384.
[34] P. Chowdhury, G. Malekshoar, M.B. Ray, J. Zhu, A.K. Ray, Ind. Eng. Chem. Res. 52 (2013) 5023–5029.
[35] Y. Zou, Z.A. Wang, X.H. Lan, N.K. Huang, C.F. Wang, J. Korean Phys. Soc. 55 (2009) 2650–2653.
[36] V. Artero, M. Chavarot-Kerlidou, M. Fontecave, Angew. Chem. Int. Ed. 50 (2011) 7238–7266.
[37] T.R. Cook, D.K. Dogutan, S.Y. Reece, Y. Surendranath, T.S. Teets, D.G. Nocera, Chem. Rev. 110 (2010) 6474–6502.
[38] L. Xu, E.M.P. Steinmiller, S.E. Skrabalak, J. Phys. Chem. C 116 (2012) 871–877.
[39] Q. Gu, J.L. Long, Y.G. Zhou, R.S. Yuan, H.X. Lin, X.X. Wang, J. Catal. 289 (2012) 88–99.
[40] D.W. Kim, S. Lee, H.S. Jung, J.Y. Kim, H. Shin, K.S. Hong, Int. J. Hydrogen Energy 32 (2007) 3137–3140.
[41] G. Sadanandam, K. Lalitha, V.D. Kumari, M.V. Shankar, M. Subrahmanyam, Int. J. Hydrogen Energy 38 (2013) 9655–9664.
[42] T.E. Feltes, L. Espinosa-Alonso, E. de Smit, L. D'Souza, R.J. Meyer, B.M. Weckhuysen, J.R. Regalbuto, J. Catal. 270 (2010) 95–102.
[43] T. De los Rios, D.L. Gutierrez, V.C. Martinez, A.L. Ortiz, Int. J. Chem. React. Eng. 3 (2005), A33, 1–9.
[44] J.G. Yu, J.R. Ran, Energy Environ. Sci. 4 (2011) 1364–1371.
[45] S. Anandan, T.N. Rao, M. Sathish, D. Rangappa, I. Honma, M. Miyauchi, ACS Appl. Mater. Interfaces 5 (2013) 207–212.
[46] B. Peng, X.W. Meng, F.Q. Tang, X.L. Ren, D. Chen, J. Ren, J. Phys. Chem. C 113 (2009) 20240–20245.
[47] J.G. Yu, S.H. Wang, B. Cheng, Z. Lin, F. Huang, Catal. Sci. Technol. 3 (2013) 1782–1789.
[48] D.L. Legrand, H.W. Nesbitt, G.M. Bancroft, Am. Mineral. 83 (1998) 1256–1265.
[49] F.L. Lu, K.H. Liao, J.M. Ting, J. Electrochem. Soc. 159 (2012) K50–K54.
[50] W.L. Xu, T.H. Lu, C.P. Liu, W. Xing, J. Phys. Chem. B 109 (2005) 14325–14330.
[51] W.J. Yang, B. Ma, W.C. Wang, Y.W. Wen, D.W. Zeng, B. Shan, Phys. Chem. Chem. Phys. 15 (2013) 19387–19394.
[52] L. Kong, Z. Jiang, H.H. Lai, R.J. Nicholls, T.C. Xiao, M.O. Jones, P.P. Edwards, J. Catal. 293 (2012) 116–125.
[53] P. Du, J. Schneider, P. Jarosz, R. Eisenberg, J. Am. Chem. Soc. 128 (2006) 7726–7727.
[54] P. Du, K. Knowles, R. Eisenberg, J. Am. Chem. Soc. 130 (2008) 12576–12577.
[55] T. Lazarides, T. McCormick, P. Du, G. Luo, B. Lindley, R. Eisenberg, J. Am. Chem. Soc. 131 (2009) 9192–9194.